Acta Mechanica Sinica (2014) 30(6):927–932
DOI 10.1007/s10409-014-0088-8

RESEARCH PAPER

The Mexican hat effect on the delamination buckling of a compressed thin film

Yin Zhang · Yun Liu

Received: 10 May 2013 / Revised: 10 December 2013 / Accepted: 25 April 2014
©The Chinese Society of Theoretical and Applied Mechanics and Springer-Verlag Berlin Heidelberg 2014

Abstract Because of the interaction between film and substrate, the film buckling stress can vary significantly, depending on the delamination geometry, the film and substrate mechanical properties. The Mexican hat effect indicates such interaction. An analytical method is presented, and related dimensional analysis shows that a single dimensionless parameter can effectively evaluate the effect.

Keywords Buckling · Delamination · Elastic foundation · Thin film · Compliant substrate

1 Introduction

For a freestanding thin film with clamped-clamped boundary conditions and a length of $2b$, the buckling load ($P_{\mathrm{c-c}}$) is given as follows [1–3]

$$P_{\mathrm{c-c}} = 4\pi^2 \frac{E_{\mathrm{f}}^* I}{(2b)^2} = \pi^2 \frac{E_{\mathrm{f}}^* I}{b^2}, \tag{1}$$

where E_{f}^* is the effective Young's modulus of the film; $E_{\mathrm{f}}^* = E_{\mathrm{f}}$ for a beam structure and $E_{\mathrm{f}}^* = E_{\mathrm{f}}/(1-\nu_{\mathrm{f}}^2)$ for a thin plate structure [1, 2]; E_{f} and ν_{f} are the film Young's modulus and Poisson's ratio. $I = ct^3/12$ (c and t are the film width and thickness, respectively). Equation (1) corresponds to the buckling scenario shown in Fig. 1a, in which there is no film/substrate interaction. Mathematically, the substrate Young's modulus (E_{s}) and Poisson's ratio (ν_{s}) have no role in the above equation. The studies on a ruck in a rug [4, 5] and a blister buckling [6] fall into this category, in which the substrate is (implicitly) assumed rigid and the clamped-clamped boundary conditions apply. However, recent studies [1–3] show that the thin film delamination buckling load can be much lower than what Eq. (1) predicts, especially for the case of a hard film on a soft substrate. When the elastic deformation of the substrate is taken into account, the film/substrate bump-like deformation profile, as shown in Fig. 1b, resembles a Mexican hat and is often analyzed by the so-called Mexican hat wavelet decomposition [2]. The boundary conditions at the delamination edges are essential for the buckling patterns [6]. The clamped-clamped boundary conditions shown in Fig. 1a requires both the displacement and the rotation at the delamination edge to be zero. In contrast, Yu and Hutchinson's analysis [3] is based on (the assumption of) nonzero displacement and rotation at the delamination edge; the clamped-clamped boundary conditions are thus violated, which leads to a lower buckling load. For a Mexican hat deformation shape, the atomic force microscope (AFM) measurement and finite element analysis (FEA) [2] show that both the displacement and the rotation are nonzero at the delamination edge. Yu and Hutchinson's free body diagram analysis is on the delamination edge and only an implicit solution can be obtained [3]. Although FEA can provide an overall analysis on this Mexican hat effect [1, 2], a great deal of insights can be gained through an analytical solution. This study shows that a dimensionless number defined as $B = 1.2(b/t)(E_{\mathrm{s}}^*/E_{\mathrm{f}}^*)^{1/3}$, which incorporates both delamination geometry and film/substrate mechanical properties, is the unique parameter responsible for the Mexican hat effect on the delamination buckling load. As the elastic foundation model is used in this study, the limitations on the model are also discussed.

The project was supported by the National Natural Science Foundation of China (11023001 and 11372321).

Y. Zhang (✉)
State Key Laboratory of Nonlinear Mechanics (LNM),
Institute of Mechanics, Chinese Academy of Sciences,
100190 Beijing, China
email: zhangyin@lnm.imech.ac.cn
Y. Liu
Faculty of Information and Automation,
Kunming University of Science and Technology,
650051 Kunming, China

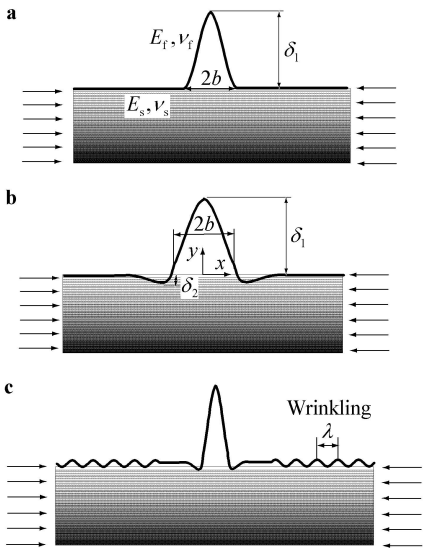

Fig. 1 **a** The buckling shape of a clamped-clamped beam/plate ($2b$ is the delamination width); **b** The Mexican hat buckling shape (δ_1 and δ_2 are the amplitudes of the delaminated and bonded zones, respectively); **c** The concomitant buckling and wrinkling (λ is the wrinkling wavelength)

2 Model development

As shown in Fig. 1, the film out-of-plane displacement, w, is divided into the following two parts [7]

$$w = \begin{cases} w_1, & -b \leqslant x \leqslant b, \\ w_2, & |x| > b, \end{cases} \tag{2}$$

where w_1 and w_2 are the displacements in the delaminated and the bonded zones, respectively, $2b$ is the delamination length, which can be caused by a pre-existing interfacial flaw or debonding by residual/external loading [1, 8]. The potential energy of the system is given as follows [9]

$$\begin{aligned} U = &\int_{-b}^{b}\left[\frac{E_f^* I}{2}\frac{w_1''^2}{1-w_1'^2} + N\left(\sqrt{1-w_1'^2}-1\right)\right]\mathrm{d}x \\ &+\int_{-\infty}^{-b}\left[\frac{E_f^* I}{2}\frac{w_2''^2}{1-w_2'^2} + N\left(\sqrt{1-w_2'^2}-1\right)+\frac{1}{2}kw^2\right]\mathrm{d}x \\ &+\int_{b}^{\infty}\left[\frac{E_f^* I}{2}\frac{w_2''^2}{1-w_2'^2} + N\left(\sqrt{1-w_2'^2}-1\right)+\frac{1}{2}kw^2\right]\mathrm{d}x, \end{aligned} \tag{3}$$

where $()' = \mathrm{d}/\mathrm{d}x$. N is the compression load applied on the thin film. The interaction between the film and the substrate is modeled as an elastic foundation and k is the elastic foundation modulus, which is given as follows [10]

$$k = 0.71E_s^*\left(\frac{E_s^* c^4}{16E_f^* I}\right)^{1/3}, \tag{4}$$

where E_s^* is the effective Young's modulus of the substrate. Using the following expansions

$$\begin{aligned} &\frac{1}{1-w'^2} = 1 + w'^2 + w'^4 + \cdots, \\ &\sqrt{1-w_2'^2} = 1 - \frac{1}{2}w'^2 - \frac{1}{8}w'^4 - \cdots, \end{aligned} \tag{5}$$

the above potential energy, U, can be approximated as

$$\begin{aligned} U = &\int_{-b}^{b}\left[\frac{E_f^* I}{2}w_1''^2(1+w_1'^2) - N\left(\frac{1}{2}w_1'^2+\frac{1}{8}w_1'^4\right)\right]\mathrm{d}x \\ &+\int_{-\infty}^{-b}\left[\frac{E_f^* I}{2}w_2''^2(1+w_2'^2) - N\left(\frac{1}{2}w_2'^2+\frac{1}{8}w_2'^4\right)\right. \\ &\left.+\frac{1}{2}kw_2^2\right]\mathrm{d}x + \int_{b}^{\infty}\left[\frac{E_f^* I}{2}w_2''^2(1+w_2'^2)\right. \\ &\left.-N\left(\frac{1}{2}w_2'^2+\frac{1}{8}w_2'^4\right)+\frac{1}{2}kw_2^2\right]\mathrm{d}x. \end{aligned} \tag{6}$$

Here the film in-plane displacement, which can have significant impacts on the film stretching energy in the post-buckling region [6, 11], is not included. This study focuses only on the buckling, on which the in-plane displacement is shown to have a minor influence [1]. The finite elasticity effect stands out only in the post-buckling region with (very) large deformation [12, 13]. By applying the principle of virtual work, i.e., $\delta U = 0$, the following governing equations are derived

$$\begin{aligned} &E_f^* I[w_1''''(1+w_1'^2) + 4w_1'''w_1''w_1' + w_1''^3] \\ &\quad +Nw_1''\left(1+\frac{3}{2}w_1'^2\right) = 0, \quad -b \leqslant x \leqslant b, \\ &E_f^* I[w_2''''(1+w_2'^2) + 4w_2'''w_2''w_2' + w_2''^3] \\ &\quad +Nw_2''\left(1+\frac{3}{2}w_2'^2\right) + kw_2 = 0, \quad |x| > b. \end{aligned} \tag{7}$$

The linearized form of Eq. (7) is as follows

$$\begin{aligned} &E_f^* I w_1'''' + N w_1'' = 0, && -b \leqslant x \leqslant b, \\ &E_f^* I w_2'''' + N w_2'' + k w_2 = 0, && |x| > b. \end{aligned} \tag{8}$$

Here $N > 0$ indicates compression. The following nondimensionalizaton scheme is introduced

$$\xi = r/a, \quad W = w/a, \quad B = b/a, \quad \Delta^2 = \frac{N}{\sqrt{4E_f^* Ik}}. \tag{9}$$

Here $a = \sqrt[4]{4E_f^* I/k}$ is called by Biot as "a fundamental length" for a beam resting on an elastic foundation [10], which is also the length used to evaluate the effect of beam bending on the contact [14]. Wagner and Vella [7] defined a length as $l_w = \sqrt[4]{E_f^* I/(\rho g c)}$ (ρ, g, and c are the fluid density, gravity acceleration and rubber sheet width, respectively) and l_w is related with the wrinkling wavelength of an elastic rubber sheet floating on a fluid. Because $\rho g c$ in the Wagner and Vella's model is the effective elastic foundation modulus k of a liquid [7], l_w is different from a only by a factor of $\sqrt{2}$. By referring to Eq. (4), a is found to be

$$a = \sqrt[4]{\frac{4E_f^* I}{k}} \approx 0.83t\left(\frac{E_f^*}{E_s^*}\right)^{1/3}. \tag{10}$$

Equation (8) is now nondimensionalized as

$$\begin{aligned} &\frac{1}{4}W_{1\xi\xi\xi\xi} + \Delta^2 W_{1\xi\xi} = 0, \qquad -B \leqslant \xi \leqslant B, \\ &\frac{1}{4}W_{2\xi\xi\xi\xi} + \Delta^2 W_{2\xi\xi} + W_2 = 0, \quad |\xi| > B, \end{aligned} \tag{11}$$

where $(\,)_{,\xi} = \mathrm{d}/\mathrm{d}\xi$ and Δ^2 is the dimensionless compression defined in Eq. (9). The solutions to Eq. (11) are given as follows [15]

$$\begin{aligned} &W_1 = A_1\cos(r_1\xi) + B_1\sin(r_1\xi) + C_1\xi + D_1, \\ &\quad -B \leqslant \xi \leqslant B, \\ &W_2 = A_2 e^{-|r_2\xi|}\cos(r_3\xi) + B_2 e^{-|r_2\xi|}\sin(|r_3\xi|) \\ &\qquad + C_2 e^{|r_2\xi|}\cos(r_3\xi) + D_2 e^{|r_2\xi|}\sin(|r_3\xi|), \\ &\quad |\xi| > B. \end{aligned} \tag{12}$$

Here $r_1 = 2\Delta$ ($\Delta > 0$), $r_2 = \sqrt{2(1-\Delta^2)}$, and $r_3 = \sqrt{2(1+\Delta^2)}$. A_i, B_i, C_i, and D_i ($i = 1, 2$) are the constants to be determined. The above solution forms are based on the assumption of $\Delta^2 < 1$, whose validity will be discussed later. The coordinate system is shown in Fig. 1b. The symmetry requirement for W_1 [1, 7, 16, 17] and the condition that W_2 needs to be finite when ξ approaches infinity give the following solutions

$$\begin{aligned} &W_1 = A_1\cos(r_1\xi) + D_1, \\ &\quad -B \leqslant \xi \leqslant B, \\ &W_2 = A_2 e^{-|r_2\xi|}\cos(r_3\xi) + B_2 e^{-|r_2\xi|}\sin(|r_3\xi|), \\ &\quad |\xi| > B. \end{aligned} \tag{13}$$

At $\xi = B$, the following matching conditions need to be satisfied [7, 17–19], which is required to ensure the continuity of displacement, slope, and moment.

$$\begin{aligned} &W_1(B) = W_2(B), \\ &W_{1\xi}(B) = W_{2\xi}(B), \\ &W_{1\xi\xi}(B) = W_{2\xi\xi}(B). \end{aligned} \tag{14}$$

Actually the matching conditions should also contain the continuity of shear force, i.e., $W_{1\xi\xi\xi}(B) = W_{2\xi\xi\xi}(B)$ [7, 17–19]. However, as the film is modeled as an infinite one, two terms in W_2 which result in infinite displacement are tossed away. Therefore, only three matching conditions are required [20]. Furthermore, it is not difficult to verify that once those matching conditions of Eq. (14) are satisfied, the shear force is continuous. By applying the above matching conditions, Eq. (13) now becomes

$$\begin{aligned} &W_1 = A_1[\cos(r_1\xi) + f_7], \\ &\quad -B \leqslant \xi \leqslant B, \\ &W_2 = A_1 e^{-r_2|\xi|}[f_8\cos(r_3\xi) + f_9\sin(|r_3\xi|)], \\ &\quad |\xi| > B. \end{aligned} \tag{15}$$

Now there is only one unknown constant, A_1, f_7, f_8, and f_9 are the parameters given in Appendix. By substituting Eq. (15) into Eq. (6) and using the symmetry condition, the system potential energy is now given as follows

$$\Pi = \frac{Ua}{E_\mathrm{f}^* I} = A_1^4(R_1 + R_2) + A_1^2(S_1 + S_2), \tag{16}$$

where Π is the dimensionless potential energy. R_1, R_2, and S_1, S_2 are the parameters given in Appendix. A_1 is determined by the energy minimization, i.e., $\partial\Pi/\partial A_1 = 0$ [17], which leads to the following equation for the buckling analysis

$$A_1[2(R_1 + R_2)A_1^2 + S_1 + S_2] = 0. \tag{17}$$

When $(S_1 + S_2)/[2(R_1 + R_2)] > 0$, $A_1 = 0$ is the only solution in the real domain; $(S_1 + S_2)/[2(R_1 + R_2)] < 0$ corresponds to three solutions. $(S_1 + S_2)/[2(R_1 + R_2)] = 0$ is thus the equation for us to tell whether the buckling occurs. For a given B, R_1, R_2, and S_1, S_2 are dependent only on Δ, as indicated in Appendix. Therefore, B is the only dimensionless parameter which has impacts on the dimensionless buckling load (Δ_c^2). From Eqs. (9) and (10), B is derived as

$$B = \frac{b}{a} = \frac{b}{0.83t}\left(\frac{E_\mathrm{f}^*}{E_\mathrm{s}^*}\right)^{-1/3} = 1.2\frac{b}{t}\left(\frac{E_\mathrm{s}^*}{E_\mathrm{f}^*}\right)^{1/3}. \tag{18}$$

3 Results and discussion

The dimensionless buckling load of a clamped-clamped thin film is given as follows

$$\Delta_{\mathrm{c-c}}^2 = \frac{P_{\mathrm{c-c}}}{\sqrt{4E_\mathrm{f}^* Ik}} = \frac{\pi^2}{4B^2}, \tag{19}$$

$P_{\mathrm{c-c}}$ is the (dimensional) buckling load as given in Eq. (1). The dimensionless buckling load (Δ_c^2) is derived from Eq. (17) by setting $(S_1 + S_2)/2(R_1 + R_2) = 0$. Figure 2 plots the variation of ratio $\Delta_\mathrm{c}^2/\Delta_{\mathrm{c-c}}^2$ as a function of B. As B increases, the ratio monotonically approaches to 1. In Parry's FEA computation [2], a Nickel film with $E_\mathrm{f} = 204\,\mathrm{GPa}$ and $\nu_\mathrm{f} = 0.312$ was deposited on a substrate, whose mechanical properties varied from a polycarbonate with $E_\mathrm{s} = 2.4\,\mathrm{GPa}$ and $\nu_\mathrm{s} = 0.37$ to a rigid one with $E_\mathrm{s} = \infty$. For a rigid substrate, the film buckling stress on a rigid substrate can be derived from Eq. (1) as $\sigma_{\mathrm{c-c}} = \pi^2 E_\mathrm{f}^*(t/b)^2/12$. For $\sigma_{\mathrm{c-c}} = 0.82\,\mathrm{GPa}$ [2], we can find that $b/t \approx 15$. For this fixed $b/t = 15$, Parry et al. [2] used the first Dundurs' elastic mismatch parameter defined as $\alpha_\mathrm{D} = (E_\mathrm{f}^* - E_\mathrm{s}^*)/(E_\mathrm{f}^* + E_\mathrm{s}^*)$, which varies from 0.98 (Nickel film on polycarbonate substrate) to -1 (rigid substrate), to study the buckling stress variation. As the first Dundurs' parameter varied from $\alpha_\mathrm{D} = 0.98$ to -1, which corresponds to B varying from 4.2 to infinity, Parry et al. showed a monotonic increase of the buckling stress, which also asymptotically approached $\sigma_{\mathrm{c-c}}$. Particularly, at $\alpha_\mathrm{D} = 0.98$ and $b/t = 15$ (corresponding to $B = 4.2$), Parry's buckling stress ratio is found to be $0.5/0.82 \approx 0.6$ and ours is $\Delta_\mathrm{c}^2/\Delta_{\mathrm{c-c}}^2 \approx 0.608$. Here the buckling load ratio is equivalent to the buckling stress ratio for a fixed cross-section. Compared with B, α_D only indicates

the mechanical difference between the film and the substrate. Yu and Hutchinson's method [3] is essentially to model the film/substrate interaction at the delamination edge by three coupled springs [1, 21]. The spring stiffnesses are dependent on b/t and two Dundurs' parameters [3]. Because the second Dundurs' parameter plays a less important role than the first one [8, 21] and $E_s^*/E_f^* = (1-\alpha_D)/(1+\alpha_D)$, the dimensionless parameter B as given in Eq. (18) is in fact a combined parameter of the geometry parameter of b/t and the elastic mismatch property of the first Dundurs' parameter. Mei et al. [8] used b/t and E_s^*/E_f^* as two independent parameters to study the buckling stress of a delaminated thin film, which shows the same asymptotic trend of the buckling stress approaching σ_{c-c}. Here the amplitude ratio of δ_2/δ_1 is used to characterize the Mexican hat effect. As shown in Fig. 1b, δ_1 and δ_2 are the amplitudes of the delaminated and the bonded parts, respectively. Figure 3 presents the amplitude ratio of δ_2/δ_1 as a function of B, in which the buckling shapes at $B = 2$ and $B = 40$ are also plotted for a comparison. The buckling shape is obtained from Eq. (13) by setting $\Delta = \Delta_c$. The ratio decreases rapidly and monotonically from $1/22$ at $B = 2$ towards 0 as B increases. In comparison, the AFM measurement yields a ratio of about $1/24$ for the post-buckling shape of a Nickel film on a polycarbonate substrate (the $B = 4.2$ case) [2].

There is an important issue needed to be addressed concerning the results presented above. As noticed in both Figs. 2 and 3, B starts from 2. Because $\Delta^2 < 1$ covers most of practical problems in the buckling analysis [15], the solution form of Eq. (13) is derived by assuming $\Delta^2 < 1$. However, Eq. (13) is incapable of analyzing the buckling of a very hard film with a chunky delamination geometry on a very soft substrate, i.e., the very small B case. For example, when $E_f^*/E_s^* = 1\,000$ and $b/t = 10$ [1], which corresponds to $B = 1.2$, we can not find Δ_c^2 in the load range of $0 < \Delta^2 < 1$. According to the Yu–Hutchinson model [3], the upper limit of the buckling load is Δ_{c-c}^2, which has already been shown in Fig. 2. As the constraints at the delamination edges relax from the clamped ones (zero displacement and rotation) to the hinged ones (zero displacement and bending moment), the buckling load reaches the lower limit of $\Delta_{c-c}^2/4$ [8]. In Fig. 2, the buckling load is 42% of Δ_{c-c}^2 at $B = 2$. Our computation can not reach this lower limit of $\Delta_{c-c}^2/4$ because there is no solution for smaller B. The solution form of Eq. (13) implicitly assumes that only delamination buckling occurs and there is no wrinkling. However, Mei et al. [8] showed that when E_s^*/E_f^* is very small (less than 10^{-3}) with relatively small b/t ratio ($b/t = 5$, 10, and 20, respectively), which corresponds to the $B < 2$ scenario, the wrinkling load/stress is smaller than that of delamination buckling. Therefore, wrinkling occurs before the delamination buckling, and the Yu-Hutchinson model becomes inapplicable [8], which implies that the lower limit is unphysical. This is the reason why Eq. (13) fails to compute the delamination buckling load when B is very small.

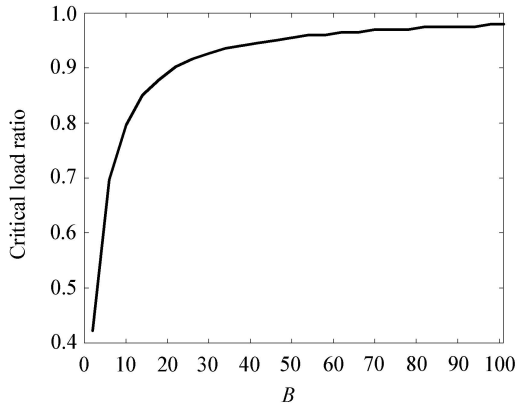

Fig. 2 The critical loads ratio ($\Delta_c^2/\Delta_{c-c}^2$) as a function of B (Δ_{c-c}^2 is the dimensionless buckling load of a clamped-clamped beam/plate)

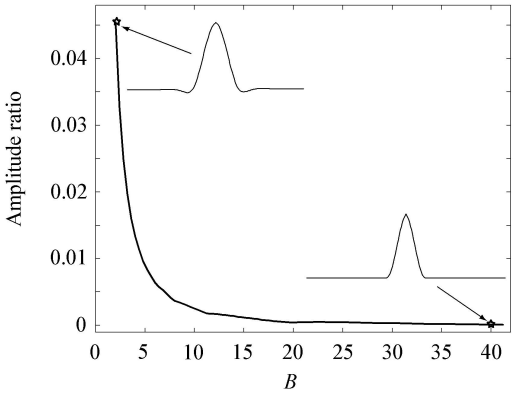

Fig. 3 The amplitude ratio (δ_2/δ_1) as a function of B. The buckling shapes at $B = 2$ and $B = 40$ are also plotted

It is also necessary for us to have some discussion on the assumptions and limitations of the model. Firstly, the reaction of substrate to thin film is modeled by the elastic foundation model, which is dependent only on the local displacement. In reality, the reaction depends on all displacements inside the substrate as indicated by the integral equation of the half space model [22]. In other words, the thin film geometry and buckling shape can influence the substrate reaction and thus k [22]. For example, the elastic foundation modulus k given in Eq. (4) is actually the one for a concentrated force acting on a substrate modeled as an elastic half space [10]. When the film wrinkles with a sine shape shown in Fig. 1c, the (effective) elastic foundation modulus is given as follows [10, 17]

$$k_w = \pi E_s^* \frac{c}{\lambda}, \tag{20}$$

where $\lambda = 2\pi t \sqrt[3]{E_f^*/(3E_s^*)}$ is the wrinkling wavelength [1]. Compared with Eq. (4), $k/k_w \approx 0.9$, there is 10% difference. There is some (minor) difference between the surface displacements in the concentrated force loading case and the Mexican hat deformation profile given by Eq. (13), and thus

the elastic foundation modulus given by Eq. (4) is expected to have some deviation from the exact one. Because an arbitrary and continuous surface displacement can be decomposed into Fourier series and each Fourier term has an effective foundation modulus as described by Eq. (20), a more accurate effective k for the Mexican hat deformation profile can be obtained by the method given by Biot [10]. However, the foundation modulus difference is expected to be minor, as corroborated by the excellent agreement of our computed buckling loads with those computed by FEA [2]. As noticed above, the foundation modulus difference between two significantly different buckling shapes is relatively small. Furthermore, the surface displacement due to a concentrated load bears some resemblance to the Mexican hat shape: Both decay rapidly with a rate proportional to $e^{-x/a}$ [10]. Secondly, if the compressive load increases further (in the post-buckling region), Δ^2 can be larger than 1. When $\Delta^2 > 1$, the following solution form holds [15]

$$\begin{aligned} W_1 &= A_1\cos(r_1\xi) + B_1\sin(r_1\xi) + C_1\xi + D_1, \\ &\quad -B \leqslant \xi \leqslant B, \\ W_2 &= A_2\cos(r_2\xi) + B_2\sin(|r_2\xi|) \\ &\quad + C_2\cos(r_3\xi) + D_2\sin(|r_3\xi|), \\ &\quad |\xi| > B. \end{aligned} \tag{21}$$

Now r_1, r_2, and r_3 change accordingly to $r_1 = 2\Delta$ ($\Delta > 0$), $r_2 = \sqrt{2\Delta^2 + 2\sqrt{\Delta^4 - 1}}$ and $r_3 = \sqrt{2\Delta^2 - 2\sqrt{\Delta^4 - 1}}$. As for $B = 1.2$, which is the case where Eq. (13) fails to compute the delamination buckling load as discussed above, FEA gives the buckling shape of the Mexican hat and then the shape of concomitant wrinkling and delamination buckling in the post-buckling region [1]. In the concomitant scenario, the Mexican hat deformation shape and sine wrinkling shape coexist as shown in Fig. 1c. Clearly, the solution form of Eq. (21) can not capture either of the buckling shapes. The possible reason is the nonlinearities of the substrate, which are mainly caused by the following three mechanisms. (1) The nonlinear strain-displacement relation. Even before the film buckling load is reached, the nonlinear Green-Lagrange strain tensor due to the finite deformation effect needs to be considered for a very soft substrate [2, 23]. (2) The nonlinear stress-strain relation of the substrate, which is characterized by the neo-Hookean constitutive law [23] or the bilinear [24] and exponential [25] elastic foundation models. (3) The fact that the substrate responds differently to tension and compression [20, 26, 27]. With an increase of compression in the post-buckling region, the nonlinear reaction of the substrate can stand out and even become dominant on the formation of buckling patterns [28, 29]. The elastic foundation model adopted here is linear and fails to incorporate these nonlinearities, which is responsible for the incapability of Eq. (21) to capture either of the shapes in the post-buckling region. Thirdly, because the elastic foundation model is introduced to study the response of the foundation surface to loads, it has the problem of accurately describing stresses [26, 30, 31]. The post-buckling stresses around the delamination edge are complex and have abrupt changes [1, 2]. Although the model includes geometrical nonlinearity of the film, it may become less accurate in the post-buckling region where there is a large compression, which requires an elastica model [7]. In the post-buckling region, the film deformation and compression can drive further delamination of the film, and mixed mode analysis of fracture mechanics is required [3, 21]. Therefore, the model is advised not to be used for the post-buckling analysis.

4 Conclusion

A model, which treats the delaminated and the bonded parts of a film as a whole, is presented to study the delamination buckling. The dimensionless parameter B is the key to analyze the delamination buckling behavior. The Mexican hat deformation shape gives a vivid image of how the film and the substrate interact, which is fully characterized by the parameter B in certain range. When B is (very) small, wrinkling may occur together with buclking; when B is (very) large, a buckling-driven delamination of film can occur, which makes B an increasing variable. The model can not handle these two scenarios. Although the model has some limitations, compared with numerical [1, 2] and implicit [3] solutions, it provides a rather straightforward and simpler analysis on the delamination buckling. The accuracy of the model is also assessed by comparing the results with those obtained in previous studies.

Appendix

The definitions of parameters

$$\begin{aligned} f_1 &= [-r_2\sin(r_3B)\cos(r_1B) + r_3\cos(r_3B)\cos(r_1B) \\ &\quad + r_1\sin(r_3B)\sin(r_1B)]/[r_3e^{-r_2B}], \\ f_2 &= \frac{-r_2\sin(r_3B) + r_3\cos(r_3B)}{r_3e^{-r_2B}}, \\ f_3 &= [r_2\cos(r_3B)\cos(r_1B) + r_3\sin(r_3B)\cos(r_1B) \\ &\quad - r_1\cos(r_3B)\sin(r_1B)]/[r_3e^{-r_2B}], \\ f_4 &= \frac{r_2\cos(r_3B) + r_3\sin(r_3B)}{r_3e^{-r_2B}}, \\ f_5 &= f_1e^{-r_2B}[(r_2^2 - r_3^2)\cos(r_3B) + 2r_2r_3\sin(r_3B)] \\ &\quad + f_3e^{-r_2B}[(r_2^2 - r_3^2)\sin(r_3B) - 2r_2r_3\cos(r_3B)], \\ f_6 &= f_2e^{-r_2B}[(r_2^2 - r_3^2)\cos(r_3B) + 2r_2r_3\sin(r_3B)] \\ &\quad + f_4e^{-r_2B}[(r_2^2 - r_3^2)\sin(r_3B) - 2r_2r_3\cos(r_3B)], \\ f_7 &= \frac{-r_1^2\cos(r_1B) - f_5}{f_6}, \\ f_8 &= f_1 + f_2f_7, \\ f_9 &= f_3 + f_4f_7, \\ f_{10} &= r_3f_9 - r_2f_8, \\ f_{11} &= -r_2f_9 - r_3f_8, \end{aligned} \tag{22}$$

$$f_{12} = -2r_2r_3 f_9 + (r_2^2 - r_3^2) f_8,$$

$$f_{13} = 2r_2r_3 f_8 + (r_2^2 - r_3^2) f_9,$$

$$g_0(\xi) = \frac{W_2(\xi)}{A_1} = \mathrm{e}^{-r_2\xi}[\, f_8 \cos(r_3\xi) + f_9 \sin(r_3\xi)],$$

$$g_1(\xi) = \frac{W_{2\xi}(\xi)}{A_1} = \mathrm{e}^{-r_2\xi}[\, f_{10} \cos(r_3\xi) + f_{11} \sin(r_3\xi)],$$

$$g_2(\xi) = \frac{W_{2\xi\xi}(\xi)}{A_1} = \mathrm{e}^{-r_2\xi}[\, f_{12} \cos(r_3\xi) + f_{13} \sin(r_3\xi)],$$

$$S_1 = \frac{1}{A_1^2} \int_0^B (W_{1\xi\xi}^2 - 4\Delta^2 W_{1\xi}^2)\mathrm{d}\xi = 4\Delta^3 \sin(4\Delta B),$$

$$S_2 = \frac{1}{A_1^2} \int_B^\infty (W_{2\xi\xi}^2 - 4\Delta^2 W_{2\xi}^2 + 4W_2^2)\mathrm{d}\xi$$

$$= \int_B^\infty (g_2^2 - 4\Delta^2 g_1^2 + 4g_0^2)\mathrm{d}\xi,$$

$$R_1 = \frac{1}{A_1^4} \int_0^B (W_{1\xi\xi}^2 W_{1\xi}^2 - \Delta^2 W_{1\xi}^4)\mathrm{d}\xi$$

$$= 4\Delta^6 \Big(\frac{B}{2} + \frac{\sin(4\Delta B)}{2\Delta} - \frac{5\sin(8\Delta B)}{16\Delta} \Big),$$

$$R_2 = \frac{1}{A_1^4} \int_B^\infty (W_{2\xi\xi}^2 W_{1\xi}^2 - \Delta^2 W_{2\xi}^4)\mathrm{d}\xi = \int_B^\infty (g_2^2 g_1^2 - \Delta^2 g_1^4)\mathrm{d}\xi.$$

References

1 Mei, H., Landis, C. Huang, R.: Concomitant wrinkling and buckle-delamination of elastic thin films on compliant substrate. Mech. Mater. **43**, 627–642 (2011)

2 Parry, G., Colin, J., Coupeau, C., et al.: Effect of substrate compliance on the global unilateral post-buckling of coatings: AFM observations and finite element calculations. Acta Mater. **53**, 441–447 (2005)

3 Yu, H.H., Hutchinson, J.W.: Influence of substrate compliance on buckling delamination of thin films. Int. J. Fract. **113**, 39–55 (2002)

4 Vella, D., Boudaoud, A., Adda-Bedia, M.: Statics and inertial dynamics of a ruck in a rug. Phys. Rev. Lett. **103**, 174301 (2009)

5 Kolinski, J., Aussillous, P., Mahadevan, L.: Shape and motion of a ruck in a rug. Phys. Rev. Lett. **103**, 174302 (2009)

6 Audoly, B.: Stability of straight delamination blisters. Phys. Rev. Lett. **83**, 4124–4127 (1999)

7 Wagner, T.J., Vella, D.: Floating carpets and delamination of elastic sheets. Phys. Rev. Lett. **107**, 044301 (2011)

8 Mei, H., Huang, R., Chung, J., et al.: Buckling modes of elastic thin films on elastic substrate. Appl. Phys. Lett. **90**, 151902 (2007)

9 Koiter, W.T.: Koiter's Elastic Stability of Solids and Structures, Edited by van der Heijden A., Cambridge University Press, New York, NY (2009)

10 Biot, M.A.: Bending of an infinite beam on an elastic foundation. J. Appl. Mech. **4**, 1–7 (1937)

11 Ziebart, V., Paul, O., Baltes, H.: Strongly buckled square micromachined membranes. J. Microelectromech. Syst. **8**, 423–432 (1999)

12 Li, B., Jia, F., Cao, Y.P., et al.: Surface wrinkling patterns on a core-shell soft sphere. Phys. Rev. Lett. **106**, 234301 (2011)

13 Li, B., Cao, Y.P., Feng, X.Q., et al.: Surface wrinkling of mucosa induced by volumetric growth: Theory, simulation and experiment. J. Mech. Phys. Solids **59**, 758–774 (2011)

14 Castillo, J., Barber, J.S.: Lateral contact of slender prismatic bodies. Proc. R. Soc. London, Ser. A **453**, 2397–2412 (1997)

15 Hetényi, M.: Beams on Elastic Foundation, The University of Michigan Press, Ann Arbor, MI (1955)

16 Vella, D., Bico, J., Boudaoud, A., et al.: The Macroscopic delamination of thin films from elastic substrate. Proc. Natl. Acad. Sci. USA **106**, 10901–10906 (2009)

17 Jiang, H., Sun, Y., Rogers, J., et al.: Post-buckling analysis for the precisely controlled buckling of thin film encapsulated by elastomeric substrates. Int. J. Solids Struct. **45**, 2014–2023 (2008)

18 Zhang, Y., Murphy, K.D.: Tensionless contact of a finite circular plate. Acta Mech. Sin. **28**, 1374–1381 (2012)

19 Zhang, Y., Murphy, K.D.: Tensionless contact of a finite beam: Cocnentrated load inside and outside the contact zone. Acta Mech. Sin. **29**, 836–839 (2013)

20 Weitsman, Y.: On foundations that reacts in compression only. J. Appl. Mech. **37**, 1019–1030 (1970)

21 Zhao, M., Yang, F., Zhang, T.Y.: Delamination buckling in the microwedge indentation of a thin film on an elastically deformable substrate. Mech. Mater. **39**, 881–892 (2007)

22 Johnson, K.L.: Contact Mechanics, Cambridge University Press, Cambridge (1985)

23 Jiang, H., Khang, D.H., Song, J., et al.: Finite deformation mechanics in buckled thin films on compliant supports. Proc. Natl. Acad. Sci. USA **104**, 15607–15612 (2007)

24 Tvergaard, V., Needleman, A.: On the localization of buckling patterns. J. Appl. Mech. **47**, 613–619 (1980)

25 Bažant, Z., Grass, P.: Size effect of cohesive delamination fracture triggered by sandwich skin wrinkling. J. Appl. Mech. **74**, 1134–1141 (2007)

26 Zhang, Y.: Tensionless contact of a finite beam resting on Reissner foundation. Int. J. Mech. Sci. **50**, 1035–1041 (2008).

27 Zhang, Y., Zhao, Y.P.: Modeling nanowire indentation test with adhesion effect. J. Appl. Mech. **78**, 011007 (2011)

28 Zhang, Y., Murphy, K.D.: Secondary buckling and tertiary states of a beam on a non-linear elastic foundation. Int. J. Nonlin. Mech. **40**, 795–805 (2005)

29 Brau, F., Vandeparre, H., Sabbah, A., et al.: Multiple-length-scale elastic instability mimics parametric resonance of nonlinear oscillators. Nature Phys. **7**, 56–60 (2011)

30 Reissner, E.: A note on deflection of plates on a viscoelastic foundation. J. Appl. Mech. **25**, 144–145 (1958)

31 Kerr, A.D.: Elastic and viscoelastic foundation models. J. Appl. Mech. **31**, 491–498 (1964)